

JGR Solid Earth

RESEARCH ARTICLE

10.1029/2024JB029002

Key Points:

- A dynamic pore network model for studying spontaneous imbibition in dual permeable media is presented
- The contrary effect of flux exchange on spontaneous imbibition within low-permeable zone under various viscosity ratios is observed
- Transition of interface dynamics from stable to unstable pattern is induced by unfavorable viscosity ratio and large permeability contrast

Correspondence to:

M. Wang,
mrwang@tsinghua.edu.cn

Citation:

Gong, W., Chen, Z., Lei, W., Zheng, J., Ju, Y., & Wang, M. (2024). Spontaneous imbibition in dual permeable media using dynamic pore network model. *Journal of Geophysical Research: Solid Earth*, 129, e2024JB029002. <https://doi.org/10.1029/2024JB029002>

Received 25 FEB 2024

Accepted 15 AUG 2024

Author Contributions:

Conceptualization: Moran Wang

Data curation: Wenhai Lei

Investigation: Wenbo Gong

Resources: Yang Ju

Supervision: Moran Wang

Validation: Zhiqiang Chen,

Jiangtao Zheng

Writing – original draft: Wenbo Gong

Writing – review & editing:

Zhiqiang Chen, Wenhai Lei,

Jiangtao Zheng, Yang Ju, Moran Wang

Spontaneous Imbibition in Dual Permeable Media Using Dynamic Pore Network Model

Wenbo Gong^{1,2} , Zhiqiang Chen³ , Wenhai Lei⁴ , Jiangtao Zheng⁵ , Yang Ju⁵ , and Moran Wang² 

¹College of Safety and Ocean Engineering, China University of Petroleum, Beijing, China, ²Department of Engineering Mechanics, Tsinghua University, Beijing, China, ³Petroleum Exploration and Production Research Institute, SINOPEC, Beijing, China, ⁴Department of Mechanics, KTH Royal Institute of Technology, Stockholm, Sweden, ⁵State Key Laboratory for Fine Exploration and Intelligent Development of Coal Resources, China University of Mining & Technology-Beijing, Beijing, China

Abstract Understanding preferential flow in porous media holds substantial theoretical significance on the design and optimization of hydrocarbon exploitation in shale reservoir. Previous researches discussed the competition of imbibition front in layered porous media while the underlining mechanism for interfacial dynamics and induced displacement efficiency of multiphase flow remains ambiguous. In this paper, we investigate the spontaneous imbibition in dual permeable media and analyze the flux exchange between the neighboring porous zones with permeability contrast using dynamic pore network model. The impact of fluid viscosity ratio and permeability contrast on the spontaneous imbibition preference have been addressed, and finally a phase diagram for displacement efficiency has been obtained. The results reveal that the dual permeable structure enhances the invasion rate of wetting fluid in the low-permeable zone and induces unstable displacement patterns, leading to reduction of the long-term displacement efficiency. The interfacial pattern transition from stable displacement to unstable pattern in dual permeable media could be ascribed into the flux exchange between dual permeable zones, which shows a contrary impact on the fluid flow within the low-permeable zone under favorable and unfavorable viscosity ratios. The permeability contrast in dual permeable media intensifies this impact during spontaneous imbibition. These results help us to understand the occurrence and mutual interaction of multiphase flow in layered porous media, and provide a theoretical guidance for the hydrocarbon exploitation in shale reservoir.

Plain Language Summary The shale oil reservoir has emerged as a crucial contributor to the global energy supply, primarily attributed to stimulation techniques such as hydraulic fracturing. The geological composition of shale rock encompasses stratified layers characterized by varying permeability, leading to diverse multiphase flow patterns at the pore scale during the shut-in period. These intricate flow patterns significantly impact shale oil recovery during subsequent exploitations. However, a gap exists in comprehending the optimal design of injection conditions by controlling the multiphase flow pattern for a high-efficiency exploitation strategy. The elucidation of multiphase displacement mechanisms within the complex porous structure featuring staggered layers are imperative. To address this gap, pore-scale modeling and analysis were conducted to visualize spontaneous imbibition behaviors across varying fluid viscosity ratios and permeability contrasts. The findings indicate that the imbibition flux in low-permeable zone is augmented by fluid flow in high-permeable zone. Furthermore, an escalating permeability contrast intensifies the flux enhancement and reduce the displacement efficiency in dual permeable media by changing the displacement pattern from stable to unstable distribution. These outcomes serve as a theoretical foundation, providing insights for the selection and optimization of an effective exploitation strategy to enhance shale oil recovery under complex engineering conditions.

1. Introduction

Multiphase flow in porous media is a ubiquitous occurrence in both natural environments and various sectors of the engineering industry, encompassing phenomena observed in soil, subsurface rock formations, and filter materials. A profound understanding of multiphase flow in porous media holds substantial theoretical and practical significance, notably guiding applications in oil and gas exploitation, contaminant transport in soil, and subsurface aqueous flow (Chen & Guo, 2023; Han et al., 2020; Mathia et al., 2019; Rothman, 1990). The inherent

characteristics of porous media introduce challenges in comprehending multiphase flow behaviors, marked by heterogeneity, nonlinearity, and multi-scale effects (Gao et al., 2021; Liu & Wang, 2020; Muljadi et al., 2016; Wang et al., 2019; Zhang et al., 2021). The diverse porous structures at various size scales within porous media exert a pronounced influence on fluid flow and the mutual interaction of multiphase fluids. Owing to large size difference, dominant processes and governing equations of fluid flow vary with scales, and it is challenging to directly capture the flow behaviors within microscopic pore structure from a macroscopic-scale model or experiment. It is more practicable by upscaling method, which allows the essence of physical processes at one level to be summarized at the coarser level (Chen et al., 2021). To the relationship of fluid flow behaviors between the microscopic and macroscopic scale, significant research efforts have been directed toward unraveling flow mechanisms, ranging from a large scale (Arshadi et al., 2018; Rothman, 1990) to the pore scale (Cieplak & Robbins, 1988, 1990; Holtzman & Segre, 2015; Hu et al., 2019; Lenormand et al., 1983; Wang et al., 2023; Zhang et al., 2011), facilitated by advancements in experimental techniques and numerical models.

Numerous pore-scale studies have focused on exploring multiphase displacement behaviors within porous media with single permeability (Lenormand et al., 1988; Rabbani et al., 2018; Wang et al., 2019), in which a representative element volume of pore structure could be specified by analyzing the permeability variation in the subdomain with different size (Liu & Wang, 2022). Previous studies underscore that the interfacial behaviors at the pore scale are influenced by a multitude of factors, including fluid properties (viscosity ratio, interfacial tension, and fluid wettability), driving conditions (pressure and velocity boundary conditions), and porous characteristics (heterogeneity, pore size distribution, and pore topology). Notably, interfacial instability at the pore scale, encompassing phenomena such as Haines jump, snap-off, cooperative pore filling, and fingering flow, has garnered increased attention due to its inherent complexity (Armstrong & Berg, 2013; Cha et al., 2021; Lei, Lu, et al., 2022; Lenormand et al., 1988). These unstable interfacial patterns often exert a profound impact on displacement efficiency in porous media, a critical parameter in the geological hydrocarbon industry. Scholars aim to discern the sensitivity of multiphase fluid displacement behaviors in porous media through comprehensive analyses, seeking optimal design strategies for maximizing displacement efficiency and offering practical recommendations for oil and gas reservoir exploitation.

It is essential to note that these investigations predominantly pertain to situations where the porous structure owns single permeability, even in the presence of heterogeneity and anisotropy (Gao et al., 2021; Lei, Lu, et al., 2023). The characterization of the porous structure in geological rocks reveals significant differences in pore size and geometry between shale rocks and conventional rocks with single permeability (Mathia et al., 2019). Shale rocks, predominantly comprising void space for hydrocarbon storage and hydrocarbon production layers, exhibit distinct pore structure characteristics in these layers. Unlike the porous structures with single permeability, the unconventional shale reservoir's basic element is the porous matrix with permeability difference (Bakhshian et al., 2020). To distinguish the structure characteristics in shale rocks, the whole pore system is considered as the combination of porous structure with larger pore size (high permeable zone) and porous structure with smaller pore size (low permeable zone), as shown in Figure 1. Therefore, the permeability contrast between high- and low-permeable zones is observed in the pore matrix. It is worth noting that the weak hydrophilic wettability is considered in this study because the shale rock is preferentially water-wet for the hydrocarbon/brine/shale system with contact angle ranging from 52° to 84° (Siddiqui et al., 2018) and the shale porous system is mostly comprise of inorganic pores with hydrophilic wettability. The displacement process of water invasion into the shale matrix during the shut-in period after hydraulic fracturing could be treated as the spontaneous imbibition, where the wetting fluid (water) is driven to displace the oil in porous media only by the capillary force. Therefore, it is imperative to study spontaneous imbibition in porous media with permeability contrast and elucidate the impact of porous structure characteristics on interfacial patterns and ultimate displacement efficiency for the shale oil recovery. Moreover, unconventional shale rocks feature a complex structure with numerous nano-scale pores and strong heterogeneity, inducing different flow mechanisms at the nano-scale, such as viscosity distribution and slip effect along the wall (Wu et al., 2017).

Research on multiphase flow in matrices with permeability contrast typically encompasses two main models: the fracture-porous medium model and the dual-permeability porous media model. The fracture-porous medium model facilitates the induction of water channels or preferential flow due to a significant difference in viscous resistance between layers with permeability contrast. Previous studies on multiphase flow in fracture-porous media indicate that fluid invasion in porous media with low permeability is driven by the pressure gradient in fractures during drainage or capillary forces during imbibition (Arshadi et al., 2018; Bakhshian et al., 2020; He

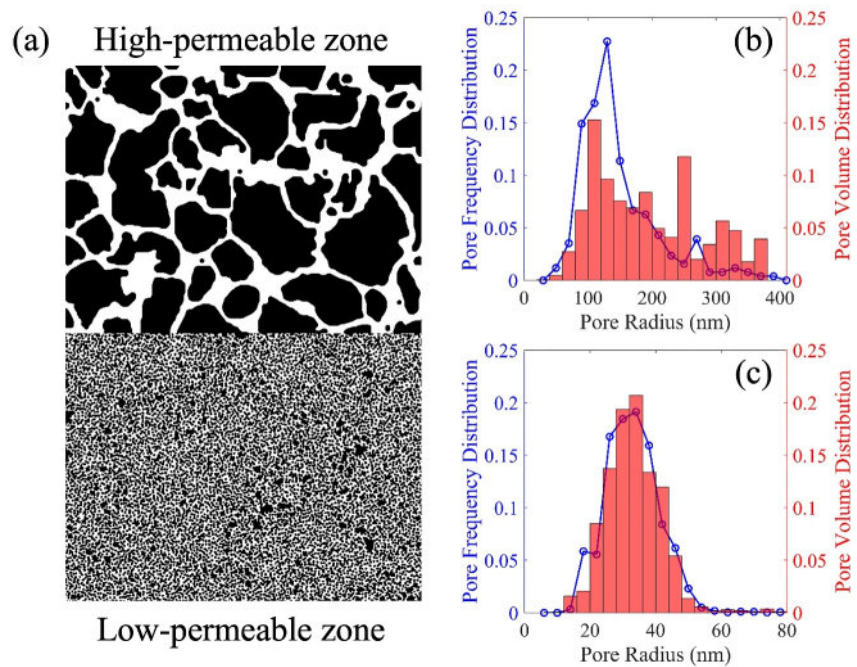


Figure 1. The structure characteristics of the dual-permeable porous media: (a) porous morphology, (b) pore size distribution in high-permeable zone, and (c) pore size distribution in low-permeable zone.

et al., 2022; Zheng et al., 2018). However, overwhelming preferential flow in fractures impedes fluid invasion in porous media with low permeability, making it challenging to uncover the mutual interaction mechanism of multiphase flow induced by multiple layers with permeability contrast (Arshadi et al., 2018). In the standard dual-permeability model, there is no communication of multiphase flow between the high- and low-permeable porous media (Choi et al., 1997). While special attention is paid to determining the mathematical model for flux exchange to ensure a logical hydrological response of mutual interaction within the layered porous system, the dual-permeability model has often been criticized as too empirical (Aguilar-López et al., 2020). Because it relies on the hydraulic conductivity that is averaged by the volumetric ratio between high- and low-permeable matrix. This approach has been found useful but physically not adequate representation of multiphase flow in a layered heterogeneous porous media (Gerke et al., 2013). Recently, another dual-permeability model, the improved pore doublet model, is applied to investigate the multiphase flow in dual permeable porous media from the pore-scale perspective, which originally represents a microscopic unit cell for studying microscopic displacement behavior (Chatzis & Dullien, 1983; Moore & Slobod, 1955). The improved pore doublet model treats the dual permeable porous media as two channels with permeability difference, one which represents porous media with higher permeability and the other one which represents a subsystem with lower permeability (Gu et al., 2021; Liu & Wang, 2022; Shan et al., 2023). However, the assumption of solid interface between dual permeable zones is made in the pore doublet model and the dual permeable porous media becomes two separated porous structures with single permeability only sharing inlet and outlet, leading to the ignoration of flux exchange in dual permeable media. The multiphase flow researches at macroscopic scale indicate that the mutual interaction between dual permeable zones plays a vital role in the total flux and multiphase distribution at final state (Huan et al., 2024). Moreover, a few pore-scale works of multiphase flow in dual permeable media shows a cooperative effect of interface dynamics between the dual permeable media (Akhlaghi Amiri & Hamouda, 2014; Lei, Li, et al., 2022), which is contractive to the traditional understanding of interfacial dynamics in single-permeability porous media (Lenormand et al., 1988). These findings all demonstrate the mutual impact between the dual permeable zones, while the multiphase flow mechanisms and mutual effects of imbibition behaviors in dual permeable media remains ambiguous at the pore scale and requires further discussion (Xie et al., 2021; Zheng et al., 2021).

The dynamic pore network model stands out among numerical methods like lattice Boltzmann method, phase-field method, and volume-of-fluid method due to its unique capacity to balance the efficiency and accuracy of the fluid flow simulation in porous media (An et al., 2020; Joekar-Niasar & Hassanizadeh, 2012). The multiphase

flow simulations in dual permeable porous media with large permeability difference often requires substantial computational resources for fine grid of porous structure (Joekar-Niasar & Hassanizadeh, 2012; Zhao et al., 2019) and become impractically complex when using these methods based on solving Navier-Stokes equations. The dynamic pore network model simplifies the complex geometry of porous structures into a network of pores and throats, allowing for more manageable computation (Chen et al., 2021). This simplification not only accelerates simulations but also facilitates a clearer understanding of the underlying physical processes (Lei et al., 2024; Lei, Gong, et al., 2023; Lei, Lu, et al., 2023; Primkulov et al., 2021; Qin et al., 2022), making the dynamic pore network model particularly valuable for applications in multiphase flow within large porous media. By capturing essential features of fluid dynamics within porous media while minimizing computational demands, the dynamic pore network model provides a practicable bridge between the microscopic mechanism and macroscopic phenomena, seeking to model and investigate the dynamic processes such as filtration, enhanced oil recovery, and groundwater remediation.

In this study, we will establish the dynamic pore network model with nanoconfinement of liquid flow capacity and explored the mutual interaction of spontaneous imbibition between the dual-permeable media with nanopores. To analyze the spontaneous imbibition behaviors and the induced hydrocarbon recovery efficiency in dual permeable media, the impact of viscosity ratio and permeability ratio on the flux exchange and interfacial patterns will be also discussed in this study. Our results will reveal the transition of interfacial patterns from stable displacement to unstable fingering patterns with varying fluid viscosity ratios and permeability ratios, which demonstrates the significant impact of flux exchange on interfacial patterns and induced displacement efficiency in dual permeable media.

2. Method and Validations

2.1. Reconstruction of Dual Permeable Porous Media

The two-dimensional porous structure was selected to investigate the spontaneous imbibition behaviors in dual permeable media owing to its intuitiveness and visualization for dynamic variation of interface patterns. The porous structure employed in this study was reconstructed using the Quartet Structure Generation Set (QSGS) method (Lei, Gong, et al., 2023), based on the essential statistical features representative of real rock microstructures. In the QSGS reconstruction of porous structure, the porosity is enlarged to enhance the connectivity of porous structure in a two-dimensional plane while the permeability is limited to be less than 1 mD. Notably, the analyzed porous media comprises two distinct components: high-permeable and low-permeable structures, characterized by average pore radii of 130 and 30 nm, respectively. To eliminate geometrical constraints on pore shapes in three-dimensional (3D) space, the dual-permeable porous media's depth is not infinite and varies spatially, corresponding to each pore's size, that is, the inscribed pore diameter. The modified 3D pore structure exhibits a consistent pore morphology in depth for each pore region. The calculated porosity and permeability are 0.31 and 550 μD , and 0.45 and 51.6 μD for high-permeable and low-permeable zones, respectively. The permeability calculation of the porous structure was conducted by lattice Boltzmann method (Chen et al., 2019). Figure 1 illustrates the porous morphology and pore size distribution for a comprehensive visualization of the analyzed structure.

2.2. Dynamic Pore Network Model

The typical procedure for a pore network model involves two primary steps: the extraction of the pore network and the subsequent modeling of multiphase flow dynamics (Blunt et al., 2002). In the context of this study, the dual-permeable porous media undergoes segmentation into numerous interconnected pore regions, as depicted in Figure 2. The corresponding porous structure is then extracted as the pore network comprising of pore body and pore throat with square cross-section utilizing the SNOW algorithm, which is achieved by balancing the hydraulic conductivity in the local pore structure with that in the combination of, as outlined by Liu et al. (2022).

There are two kinds of approaches to describe multiphase flow in pore network: the quasi-steady and dynamic pore network models. Different from the quasi-steady model that only depends on the local capillary force (i.e., the entry capillary pressure), the dynamic pore network model is capable of balancing the capillary and viscous forces, where the interface invasion is controlled by the capillary force and the transient flux are governed by the competition between the local viscous force and capillary force (Joekar-Niasar & Hassanizadeh, 2012). In this study, the dynamic pore network model is used to simulate the spontaneous imbibition in dual-permeable porous

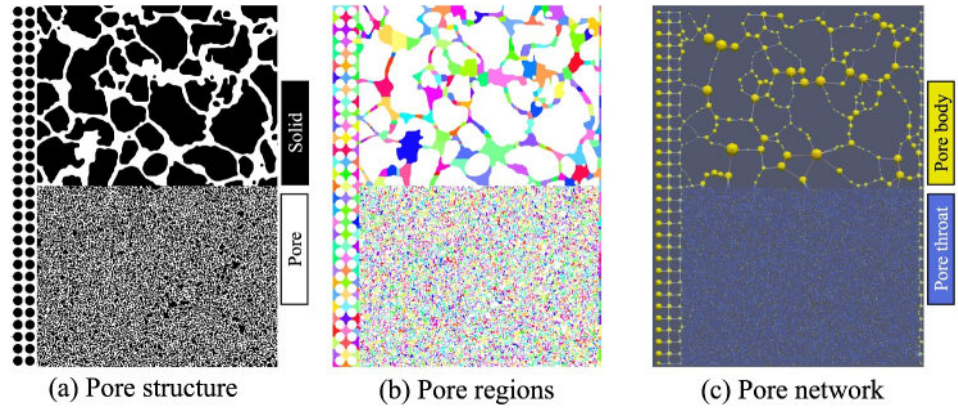


Figure 2. Pore network extraction of dual-permeability media. The color parts in subfigure (b) represent different pore regions. Two layers with large pore space are connected to the porous matrix at the inlet and outlet.

media for the Newtonian, incompressible, and immiscible fluids. The mass conservation of incompressible multiphase flow in a pore body i requires:

$$V_i \frac{\partial S_{\alpha,i}}{\partial t} + \sum_j Q_{\alpha,ij} = 0 \quad (1)$$

$$\sum_j (Q_{w,ij} + Q_{n,ij}) = 0 \quad (2)$$

where $S_{\alpha,i}$, V_i are the fluid saturation of phase α and pore volume in the pore body i ($\alpha = w, n$ stand for the wetting and nonwetting fluids). $Q_{\alpha,ij}$ is the volumetric flux of phase α through the pore throat ij connected to the pore body i and pore body j , which is given by:

$$Q_{\alpha,ij} = K_{\alpha,ij} (P_{\alpha,i} - P_{\alpha,j}) \quad (3)$$

where $P_{\alpha,i}$ and $P_{\alpha,j}$ are the fluid pressure of phase α in the pore body i and j . $K_{\alpha,ij}$ denotes the equivalent hydraulic conductivity as a function of the pore throat area A , pore throat length L and fluid viscosity μ_α . Herein, only the main-meniscus displacement occurs in the square cross-section (half angle $\beta = \pi/4$) with weak hydrophilic wettability (contact angle $\theta = 60^\circ$), and the corner flow is suppressed because of the geometrical limitation of contact angle ($\theta + \beta > \pi/2$) (Øren et al., 1998). For the creeping isothermal flow, the fluid conductivity could be described as (Patzek & Silin, 2001):

$$K_{\alpha,ij} = \chi GA^2 / \mu_\alpha L \quad (4)$$

where $\chi (=0.5623)$ is the conductivity coefficient for the square cross-section, and $G (=1/16)$ is the shape factor of the square cross-section (Patzek & Silin, 2001). To establish the dynamic pore network model of spontaneous imbibition in nano-scale porous media, the nanoconfinement of liquid flow capacity induced by an interaction from nanopore walls (Wu et al., 2017, 2019) is considered. The hydraulic conductivity of fluids in nanopores is modified based on the impact of slip length and spatial variation of confined fluid viscosity in the dynamic pore network model.

$$K_\alpha^{nano} = K_\alpha * \left(1 + \frac{4l_{s,t}}{r} \right) \frac{\mu_\alpha}{\mu_\alpha^{eff}} \quad (5)$$

where $l_{s,t}$ are the slip length of multiphase fluids along the nanopore wall:

$$l_{s,t} = \begin{cases} 0.41/(\cos \theta + 1)^2 & \text{for wetting phase} \\ \delta(\mu_{\alpha}^{ad}/\mu_{\alpha} - 1) & \text{for nonwetting phase} \end{cases} \quad (6)$$

and δ is the average distance between the adjacent layer of oil molecules (Wu et al., 2019). μ_{α}^{eff} and μ_{α}^{ad} are the effective viscosity of multiphase fluids and the corresponding viscosity in the adsorbed zone within nanopores:

$$\mu_{\alpha}^{eff} = \mu_{\alpha}^{ad} \frac{A_{ad}}{A} + \mu_{\alpha} \left(1 - \frac{A_{ad}}{A}\right) \quad (7)$$

$$\frac{\mu_{ad}}{\mu_{\infty}} = \begin{cases} -0.018\theta + 3.25 & \text{for wetting phase} \\ \tau \exp[S\alpha\sigma_1(1 - \cos\theta)/kT] & \text{for nonwetting phase} \end{cases} \quad (8)$$

where τ is the natural relaxation time describing the mutual effect strength between the nonwetting phase (n-alkanes) and solid wall, S is the equivalent wall area of a hole into which a neighboring molecule can move, α is the proportion of the equivalent wall area constituted of a solid wall, σ_1 is the surface tension of the n-alkanes in a vacuum, θ is the contact angle for the n-alkanes on the solid surface in a vacuum, T is temperature, and k is the Boltzmann constant.

For the multiphase flow in a tube with angular cross-section, the geometrical limitation on interface curvature of multiphase fluids requires that the arc-meniscus occurs only under $\theta + \beta < \pi/2$, and the main-meniscus happens under $\theta + \beta \geq \pi/2$, where β is the half angle of the cross-section corner. In this study, the entry capillary pressure of pore throat ij with square cross-section ($\beta = \pi/4$) is described based on the interfacial patterns (Øren et al., 1998):

$$P_{c,entry} = \begin{cases} \frac{\gamma}{R} \left(\cos \theta + \sqrt{\frac{\pi}{4} - \theta + \sin \theta \cos \theta} \right) & \left(\theta < \frac{\pi}{4} \right) \\ \frac{2\gamma \cos \theta}{R} & \left(\theta \geq \frac{\pi}{4} \right) \end{cases} \quad (9)$$

Accounting for the curvature variation in the main-meniscus filling event during imbibition invasion from throats to pores, the relationship between the local capillary pressure and wetting-phase saturation is modified based on the previous model (Qin & van Brummelen, 2019):

$$P_c = \frac{2\sigma \cos \theta}{R_{inter}}, \quad R_{inter} = \begin{cases} \min\{R_{t,ij}\} & S_w < 0.04 \\ \max\{R_{t,ij}\} & 0.04 \leq S_w < 0.1 \\ R_b & 0.1 \leq S_w < 0.96 \\ R_b \left(\frac{S_w - 1}{1 - 0.96} \right)^4 & S_w \geq 0.96 \end{cases} \quad (10)$$

In the simulation of dynamic pore network model, the fully implicit scheme usually brings about small time interval for transient process and costs considerable computational resources, and the IMP-SIMS (implicit pressure semi-implicit saturation) scheme could result in numerical errors under certain conditions due to the approximation of capillary pressure difference by one-order Taylor expansion (Chen et al., 2020). Both the explicit and semi-implicit update schemes will lead to global mass conservation errors in the pore network (Qin et al., 2019). In this study, we solve the governing equations (Equation 1) separately for unknown variables $P_{n,i}$ and $S_{w,i}$ in each pore body using the implicitly approach. The corresponding discrete scheme is described as:

$$\frac{V_i}{dt}(S_{w,i}^{t+1} - S_{w,i}^t) + \sum_j \left[\frac{K_{w,ij}^t}{K_{w,ij}^t + K_{n,ij}^t} (Q_{w,ij}^t + Q_{n,ij}^t) - \frac{K_{w,ij}^t K_{n,ij}^t}{K_{w,ij}^t + K_{n,ij}^t} (P_{c,i}^{t+1} - P_{c,j}^{t+1}) \right] = 0 \quad (11)$$

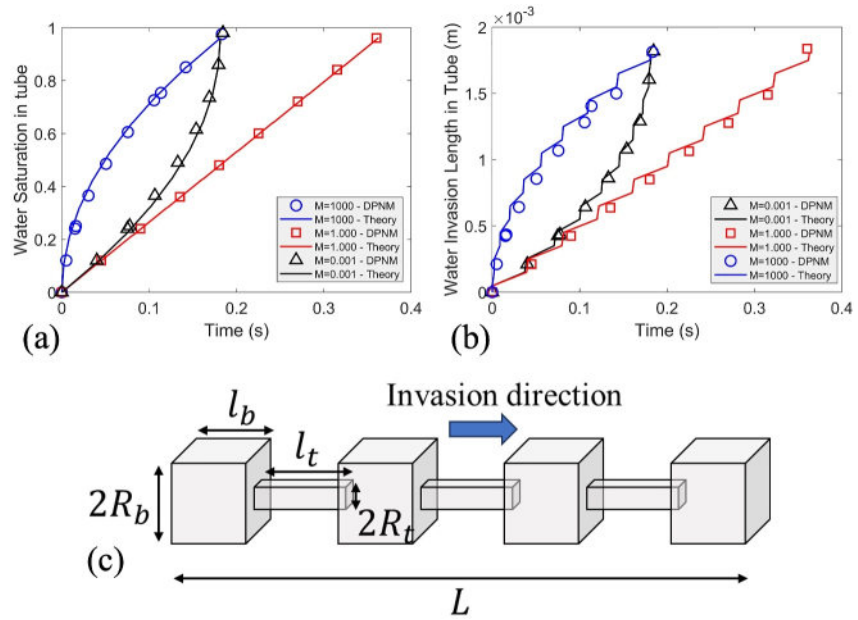


Figure 3. Validation of spontaneous imbibition in a single square tube with various cross-section: (a) temporary variation of water saturation; (b) temporary variation of water invasion length; (c) schematic diagram of pore network. $M = \mu_w/\mu_n$ is the viscosity ratio of invading phase and defending phase. DPNM is our new dynamic pore-network model.

$$\sum_j Q_{w,ij} + Q_{n,ij} = \sum_j [K_{w,ij}^t ((P_{n,i}^{t+1} - P_{c,i}^t) - (P_{n,j}^{t+1} - P_{c,j}^t)) + K_{n,ij}^t (P_{n,i}^{t+1} - P_{n,j}^{t+1})] = 0 \quad (12)$$

The local capillary pressure in each pore body is solved as a function of wetting-fluid saturation in the Newtonian iteration using the Automatic differentiation method, which is helpful to control the saturation variation during the displacement process.

To ascertain the precision of the dynamic pore network model, we conducted simulations of spontaneous imbibition within a square tube with varying cross-sections. The tube employed in the modeling consists of identical elements, namely pore bodies and throats, with the pore radius being three times that of the throat radius. For reference, the analytical solution for spontaneous imbibition in a tube with axial variation can be found in Appendix A. As depicted in Figure 3, a comparison between the results obtained from dynamic pore network modeling and the analytical solutions reveals a close match in the temporary variation of both water saturation and the length of water invasion during spontaneous imbibition. This alignment demonstrates the accuracy of the dynamic pore network model in capturing the essential dynamics of spontaneous imbibition in the tube with varying cross-sections. Moreover, the dynamic pore network model in this work is validated by comparison of interfacial pattern and saturation variation extracted from experimental and numerical researches during imbibition process within a heterogeneous pore structure, as shown in Appendix B.

3. Results and Discussion

3.1. The effect of Dual Permeable Media on Spontaneous Imbibition

3.1.1. The Interfacial Dynamics in Porous Media

We conducted a series of pore-scale simulations to investigate spontaneous imbibition in porous media, employing the dynamic pore network model. Considering the viscosity difference of fluids in the shale reservoir such as high viscosity ratio for water-gas system and low viscosity ratio for water-oil system, we varied the fluid viscosity ratio across a range from 0.02 to 50, while maintaining a fixed nonwetting-fluid viscosity of 1 mPa·s in the simulations. The boundary conditions at both the inlet and outlet were set as zero-pressure boundary conditions. Initially, the wetting fluid occupied the first-layer pores at the inlet, and the remaining pores within the porous media were saturated by the nonwetting fluid. To examine the effect of flux exchange between the dual permeable porous media

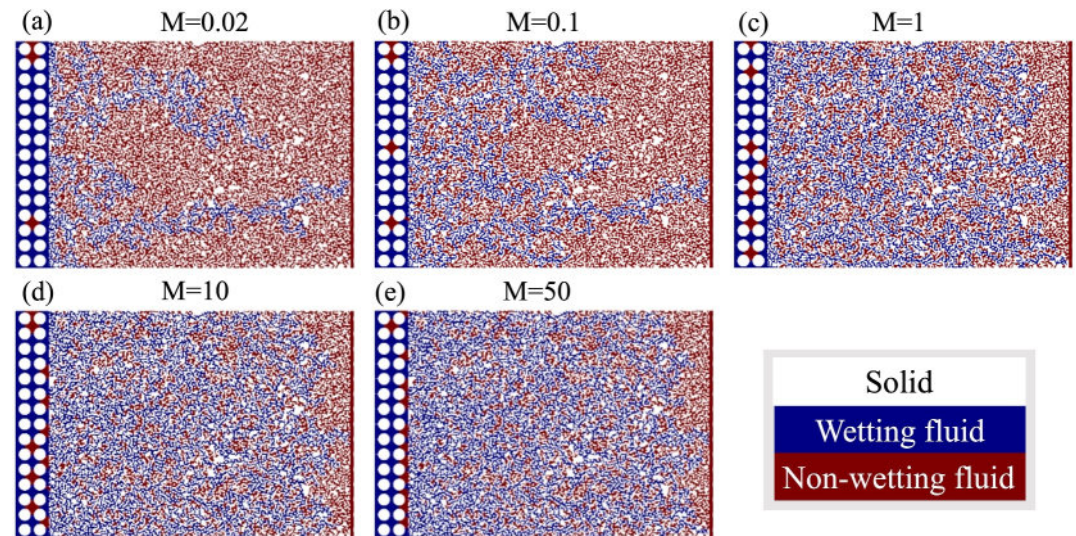


Figure 4. The spatial distribution of immiscible fluids at breakthrough state: (a–e) stand for different simulation cases where the viscosity ratios are 0.02, 0.1, 1, 10, 50.

on the interfacial dynamics in low permeable matrix, two distinct numerical conditions were employed in this study, one which simulates the spontaneous imbibition in dual permeable media, and the other one in which the solid interface is applied between the dual permeable zone. For simplification, only the spontaneous imbibition in the single-permeable media (low permeable zone) is simulated for the latter condition.

In the context of spontaneous imbibition within single-permeable media, the interfacial pattern is governed by the interplay between viscous and capillary forces. Illustrated in Figure 4 is the spatial distribution of immiscible fluids as the wetting fluid reaches the outlet pore. The outcomes reveal that, at low viscosity ratios (unfavorable condition), the wetting fluid exhibits a fingering pattern, while at high viscosity ratios (favorable condition), a stable displacement pattern emerges. This behavior is attributed to the increasing dominance of viscous resistance over capillary forces as the viscosity ratio rises. Consequently, interfacial instability, characterized by viscous fingering, is induced within the porous media. This observation aligns with findings from prior research (Lenormand et al., 1988).

The quantitative examination of the viscosity ratio's impact on spontaneous imbibition is elucidated in Figure 5. We introduce an additional fluid topology metric, the Euler number, that is, $\chi = \beta_0 - \beta_1 + \beta_2$ (where β_0 is the number of objects, β_1 is the number of redundant loops and β_2 is the number of cavities), which is an index of the flow pathway morphology as the discrete flow pathway or uniform network pathway. The Euler number of wetting-phase in porous media is calculated to represent the complexity of the interface pattern of multiphase fluids at the breakthrough state. In Euler number calculations, consideration is limited to pore space where the wetting-fluid saturation exceeds 0.5, utilizing the Fiji plugin MorphoLibJ (Legland et al., 2016). Wetting-fluid saturation is computed by summing the volume of wetting fluid in each pore, expressing its ratio to the total volume of wetting fluid in relation to the entire porous system. Figure 5a illustrates a monotonic decrease in the Euler number induced by the increasing viscosity ratio, which reflect a transition of interfacial pattern from unstable fingering distribution under low viscosity ratio to a compact invasion pattern under high viscosity ratio. At higher viscosity ratios, the fingering instability of the wetting fluid is suppressed, and the interfacial pattern tends toward stable displacement, resulting in an increased wetting-fluid saturation. It is noteworthy that the heightened viscosity of the wetting fluid translates to increased viscous resistance, while the capillary force remains constant as the driving force. Consequently, the wetting fluid invades the porous structure at a lower velocity, requiring more time to complete the immiscible displacement process during spontaneous imbibition, as depicted in Figure 5b.

Furthermore, we conduct an assessment of the nonwetting-fluid flux in the outlet pores at the breakthrough state, illustrated in Figure 5c. The spatial arrangement of outlet pores in single-permeable media is portrayed in Figure 5d. The numerical results indicate that, under higher viscosity ratios, the curve of nonwetting-fluid flux in the outlet

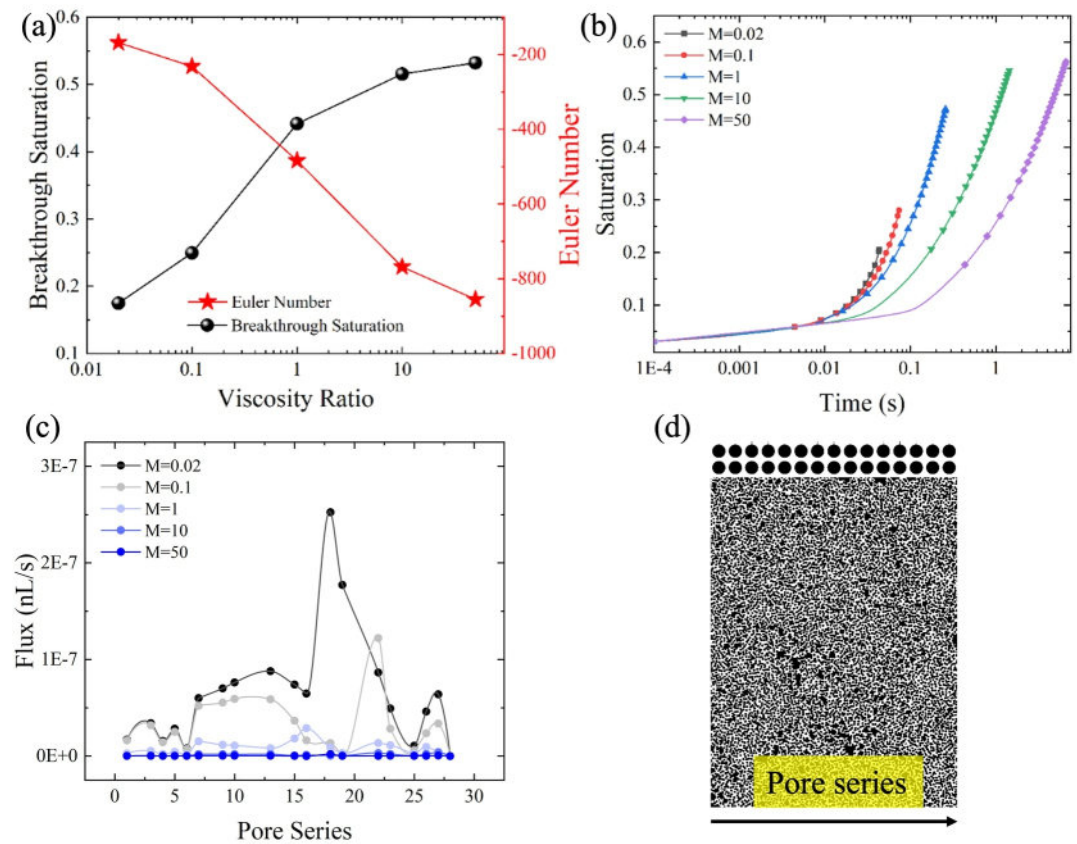


Figure 5. The statistical characteristics of spontaneous imbibition in one-permeable media: (a) Effect of viscosity ratio; (b) water saturation variation; (c) Flux distribution in outlet pores; (d) Diagram of pore series at outlet.

pores tends toward a plateau. This observation underscores that increased viscous resistance restrains multiphase flow during spontaneous imbibition in single-permeable media.

The spatial distribution of multiphase fluids in dual-permeable media at breakthrough state under various viscosity ratios is depicted in Figures 6a–6e. The breakthrough state denotes the transient time when the wetting fluid reaches the outlet pores located in the low-permeable zone of dual-permeable media. Analogous to the observations of spontaneous imbibition in single-permeable media, the wetting fluid exhibits a fingering pattern under lower viscosity ratios and a stable pattern under higher viscosity ratios. However, in dual-permeable media, the interfacial pattern is interfered by the fluid flux through the high-permeable zone. Regardless of the viscosity ratio, the wetting fluid tends to invade the pores close to the high-permeable zone. Even in cases of stable displacement with a favorable viscosity ratio, higher viscosity of wetting fluid weakens the differences between imbibition behaviors in pores near and far from the high-permeable zone, as indicated by the black arrows in Figures 6c–6e. Conversely, for fingering displacement in cases with an unfavorable viscosity ratio, the fingering pattern in pores close to the high-permeable zone intensifies, leading to significant differences in invasion patterns within the low-permeable zone of dual-permeable media.

Examining the temporary variation of wetting-fluid saturation in Figures 6f–6j, it is observed that the variation of wetting-fluid saturation in dual-permeable media consistently occurs more rapidly than that in single-permeable media. Notably, the discussed wetting-fluid saturation represents the invasion percentage of the wetting fluid in the low-permeable zone. The comparison of temporary variations in fluid saturation demonstrates that the velocity of spontaneous imbibition in the low-permeable zone is enhanced by the fluid flux in the high-permeable zone. Furthermore, due to differences in displacement patterns induced by viscosity ratios, wetting-fluid saturation is reduced under lower viscosity ratios and enhanced under higher viscosity ratios. In Figure 7, we present statistical results at the breakthrough state under various viscosity ratios, encompassing wetting-fluid saturation (S_w), Euler number (Eu), and breakthrough time. These quantitative results exhibit a similar variation induced by viscosity

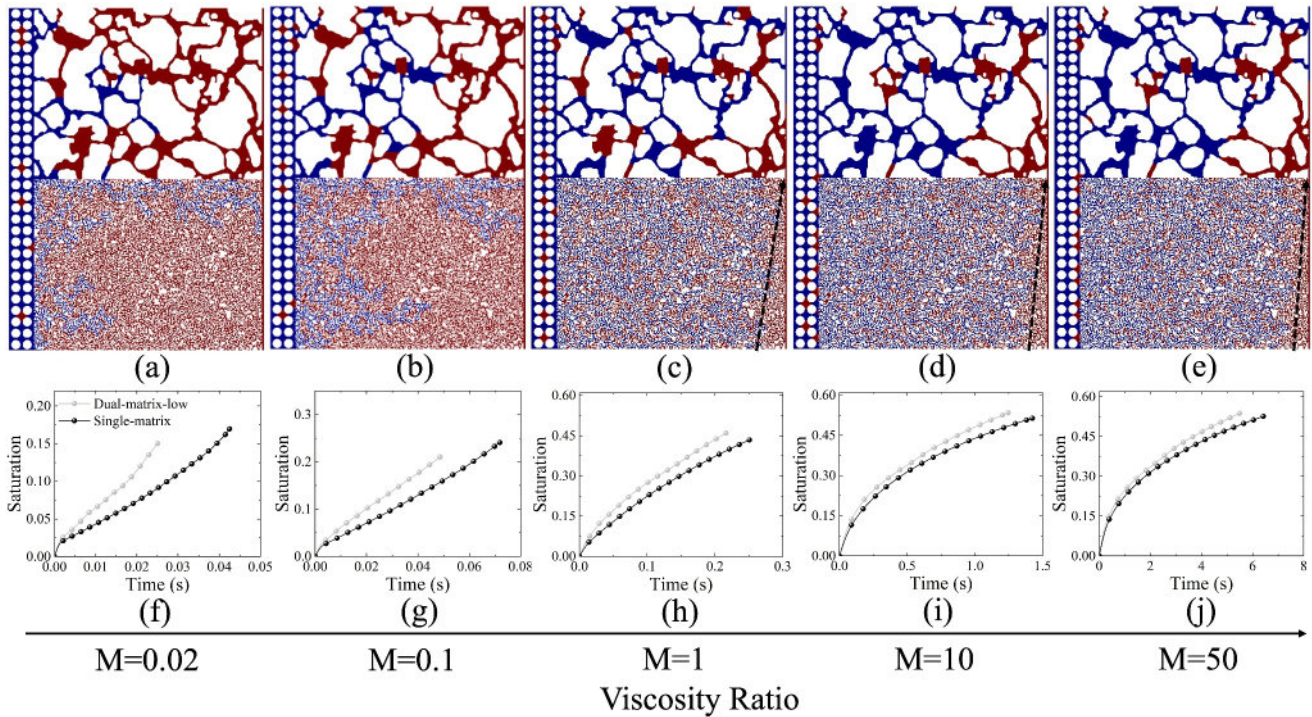


Figure 6. The interfacial pattern during spontaneous imbibition at breakthrough state (a–e), and temporary variation of water saturation before breakthrough state (f)–(j). The dual-matrix-low represents the saturation variation in the low permeable zone under the condition of dual permeable porous media, and the single-matrix for the condition of single permeable media.

ratio during spontaneous imbibition in single- and dual-permeable media, but a contrary impact on the interfacial pattern and wetting-fluid saturation.

3.1.2. The Flux Exchange in Dual Permeable Media

The visualized and quantitative data from spontaneous imbibition in porous media highlight the discernible influence of fluid flux in the high-permeable zone on the imbibition dynamics within the low-permeable zone. This influence manifests differently in terms of the interfacial pattern and fluid saturation. However, the fundamental mechanism governing spontaneous imbibition in the low-permeable zone of dual-permeable media remains elusive. Existing models for multiphase flow in dual-permeable media operate under the fundamental assumption that there is no flux exchange between the low- and high-permeable zones, with both zones sharing the same inlet and outlet regions. While this model effectively predicts the preferential sequence by balancing local viscous and capillary forces between the dual-permeable media, it falls short in capturing the flux variation in dual permeable zones and its impact in spontaneous imbibition behaviors.

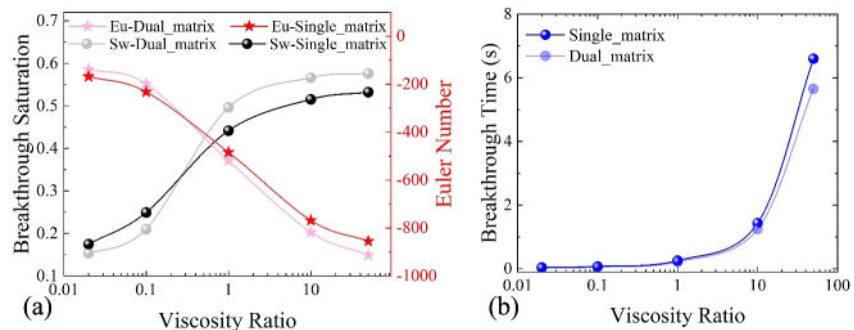


Figure 7. The effect of viscosity ratio on spontaneous imbibition in dual-permeable media.

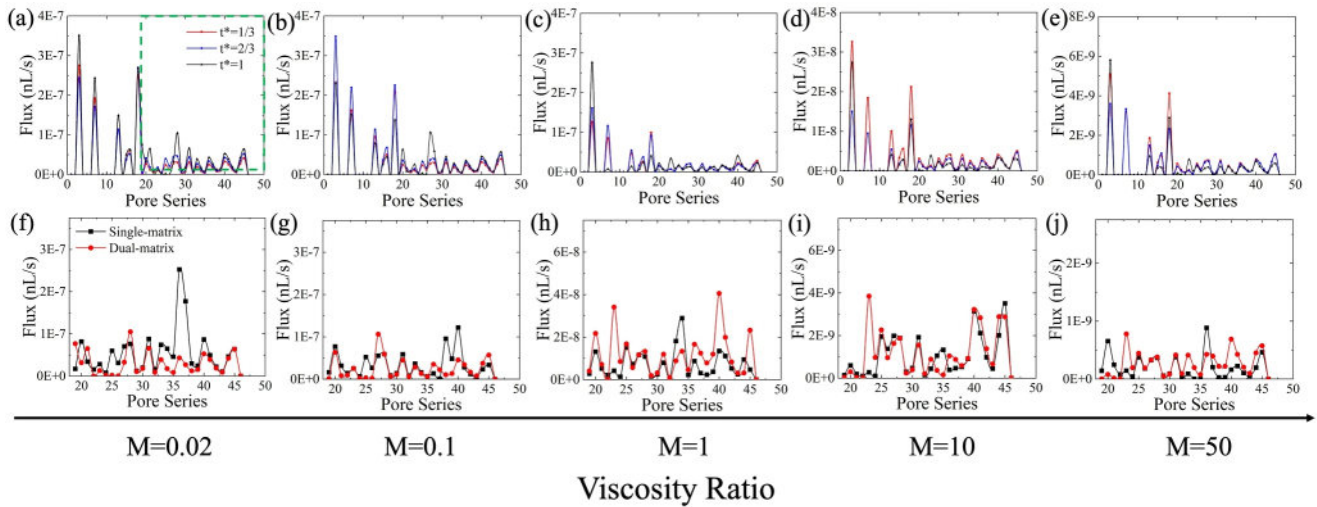


Figure 8. The nonwetting-fluid flux at breakthrough state in the outlet pores of dual permeable media (a–e), and comparison of nonwetting-fluid flux in the outlet pores between one-permeable media and low-permeable zone of dual-permeable media (f–j). Viscosity ratio varies from $M = 0.02$ to $M = 50$.

In this study, we label the breakthrough time t_0 as $t^* = 1$, when the water front invades the outlet pores in low permeable zone. Additionally, we examine the transient states of spontaneous imbibition at two other times $t_0/3$ and $2t_0/3$, that is, $t^* = 1/3$ and $t^* = 2/3$, as illustrated in Figures 8a–8e. The horizontal axis (*Pore series*) represents the series of pores at the outlet in dual-permeable media, with pore numbers 1–18 corresponding to the outlet pores in the high-permeable zone and pore numbers 19–46 representing the outlet pores in the low-permeable zone. Across various viscosity ratios ($M = 0.02, 0.1, 1, 10, 50$), the nonwetting flux in high-permeable zone at different transient states ($t^* = 1/3, 2/3, 1$) consistently exceeds that in the low-permeable zone. This observation seems to indicate that the fluid flux in the low-permeable zone will be always enhanced with the impact of fluid flux in high-permeable zone with larger fluid flux. However, the comparison of nonwetting-fluid flux in the outlet pores of the low-permeable zone reveals distinct behavior depending on the viscosity ratio, as shown in Figures 8f–8j. Specifically, the nonwetting flux in low-permeable zone is suppressed during the spontaneous imbibition in dual permeable media. The nonwetting-fluid flux in dual-permeable media is generally lower than that in single-permeability media when the viscosity ratio is smaller than 1 ($M < 1$), while in dual-permeable media, it is higher when the viscosity ratio is greater than or equal to 1 ($M \geq 1$). This observation is further supported by a comparison of the total flux between single- and dual-permeable media in Figure 9.

To comprehend the variation in total flux within the low-permeable zone under various viscosity ratios, we scrutinize the flux exchange between the low- and high-permeable zones, induced by the fluid pressure difference. Consequently, we establish a simplified model incorporating dual permeability to analyze fluid pressure under low and high viscosity ratios. As illustrated in Figure 9, the simplified model encompasses dual permeable

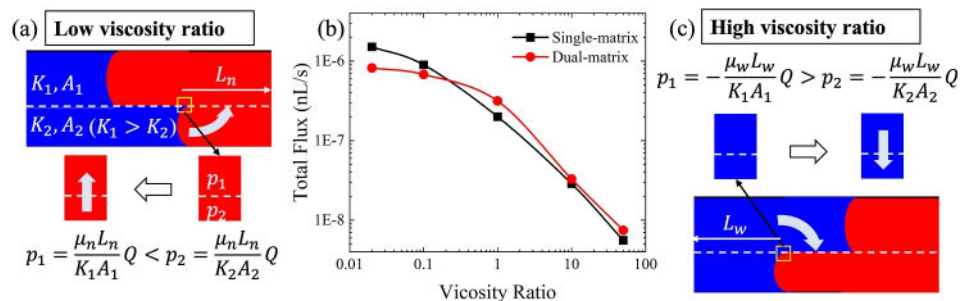


Figure 9. The flux exchange between high permeable and low permeable zone in dual-permeable porous media during spontaneous imbibition.

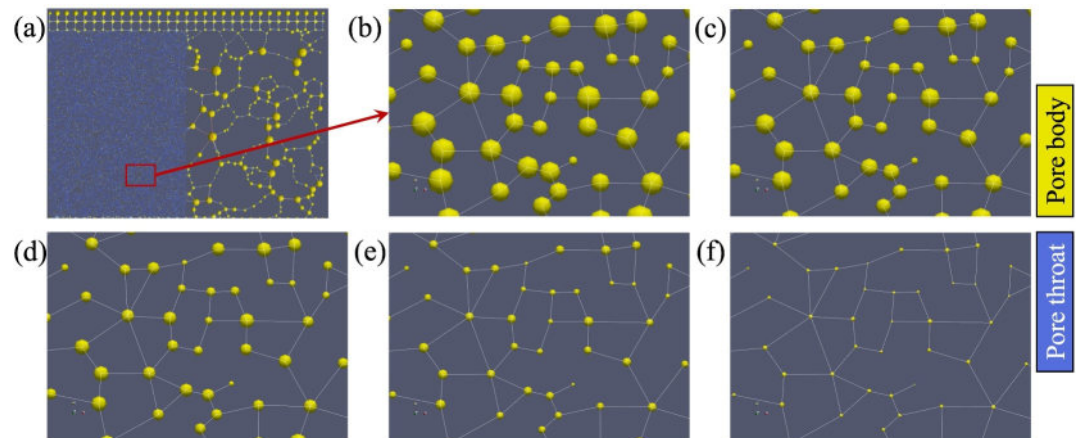


Figure 10. The schematic diagram of pore networks with various sizes and identical pore topology. The size ratios in subfigures (b)–(f) are 1.0, 0.8, 0.6, 0.4, and 0.2, respectively.

zones with permeabilities and cross-sectional areas denoted as K_1 and A_1 for the high-permeable zone and K_2 and A_2 for the low-permeable zone ($K_1 > K_2$ and $A_1 > A_2$).

Under a low viscosity ratio ($M = 0.02$), where viscous resistance dominates, the flux exchange is primarily controlled by nonwetting fluid, and their pressures in different permeable zones are evaluated using Darcy's law: $p_1 = \mu_n L_n Q / K_1 A_1$ and $p_2 = \mu_n L_n Q / K_2 A_2$ (where L_n is the distance between the fluid node and the outlet). The fluid pressure is assumed to be zero at the inlet and outlet during spontaneous imbibition. With the resultant pressure difference between the low- and high-permeable zones, nonwetting fluid flows from the low-permeable zone to the high-permeable zone (Figure 9a), leading to a decrease in the nonwetting-fluid flux into the outlet of the low-permeable zone. Consequently, the nonwetting-fluid flux in the low-permeable zone is suppressed in dual-permeable media under low viscosity ratios due to the flux into the high-permeable zone. Similarly, when viscous resistance is primarily attributed to the wetting fluid under a high viscosity ratio ($M = 50$), the wetting fluid flows from the high-permeable zone to the low-permeable zone under pressure difference, resulting in an enhanced flux into the outlet of the low-permeable zone. While the simplified model with dual permeability qualitatively explains the flux exchange between the low- and high-permeable zones, a quantitative model is essential for further analysis in future research.

3.2. The Effect of Permeability Ratio in Dual Permeable Media

3.2.1. The Effect of Permeability Ratio on Displacement Pattern

The aforementioned findings have illustrated that the variation in viscous resistance leads to differences in flux exchange within dual-permeable media. The resulting displacement behaviors during spontaneous imbibition were discussed across a range of viscosity ratios. In this section, we delve into the interplay between capillary force and viscous force within dual-permeable media, focusing specifically on the influence of permeability ratio. To introduce variations in permeability, we manipulate the pore size within the original pore network while preserving the same pore topology. Notably, we maintain a fixed throat length in the modified pore networks to align with the geometric dimensions of the high-permeable zone. The local distribution of pore-throat in the modified pore networks is showcased in Figures 10b–10f, where the size ratios of pores in the modified networks to that of the original one are 1.0, 0.8, 0.6, 0.4, and 0.2.

Table 1
The Pore Structure Information of the Designed Pore Networks

Pore size ratio	1.0	0.8	0.6	0.4	0.2
Average pore radius (nm)	30	24	18	12	6
Porosity	0.39	0.2	0.084	0.025	0.0031
Permeability (μD)	57.5	34.6	15.8	4.17	0.29

Table 1 and Figure 11p present the porosity and permeability values of the modified pore networks. The permeability of the original pore network, calculated using a pore-network model, closely approximates the value determined by the lattice Boltzmann method, with a relative error of 11.4%. The permeability across the modified pore networks exhibits a substantial variation, ranging from 57.5 μD to 0.29 μD . This variability allows us to

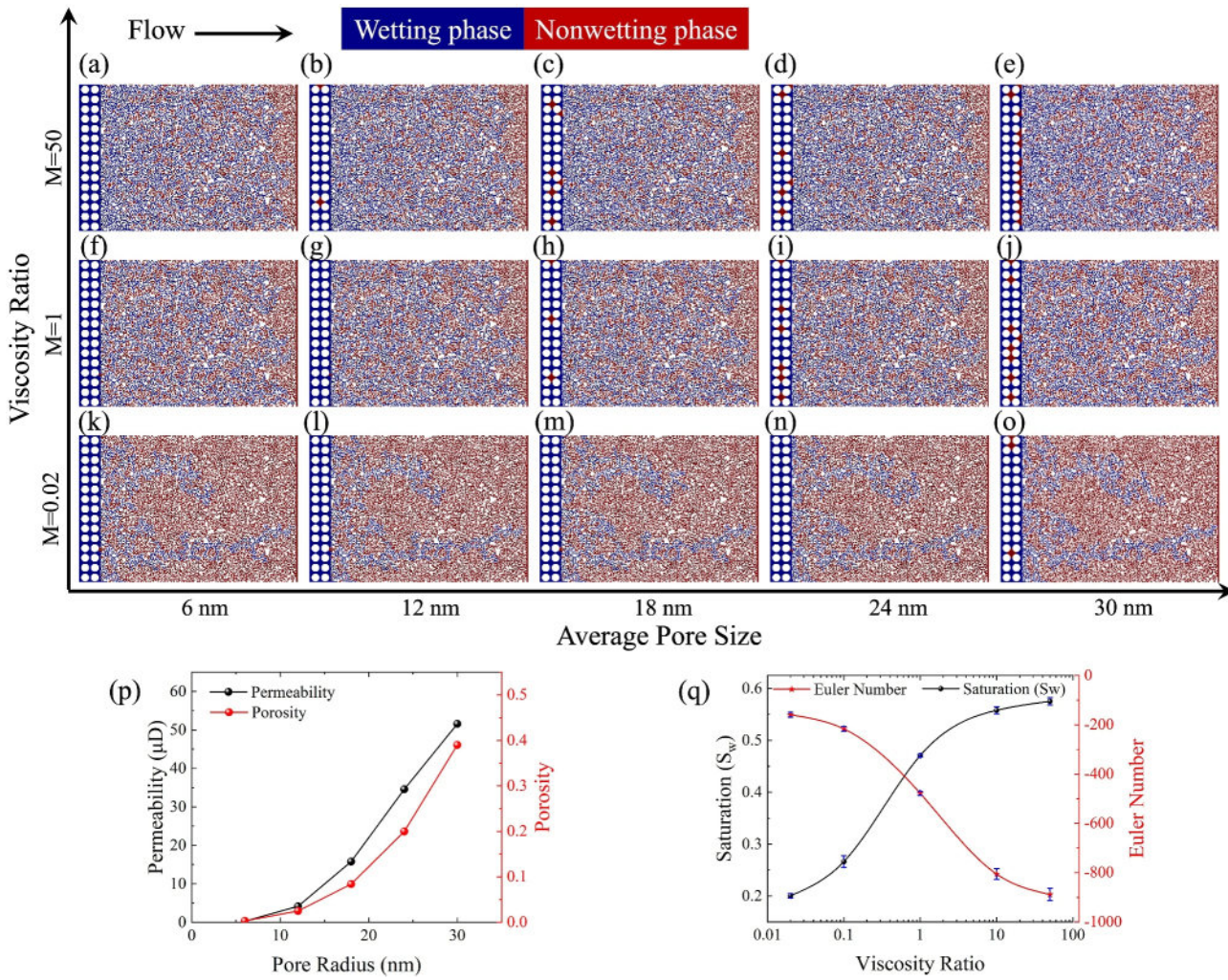


Figure 11. The modeling results of spontaneous imbibition in one permeable media using dynamic pore network model under various permeability ratios and pore sizes. (a–o) are the spatial distribution of immiscible fluids at breakthrough state in the modified pore networks with various average pore radii under different viscosity ratios, (p) is the pore structure information for the modified pore networks, (q) depicts the variation of saturation and Euler number of wetting fluid under various pore sizes.

analyze the impact of flux exchange in dual-permeable media arising from changes in viscous resistance induced by the permeability ratio between the low- and high-permeable zones.

In the context of spontaneous imbibition, the invasion of wetting fluid is contingent upon the equilibrium between local viscous and capillary forces, both of which are influenced by pore size. Utilizing the dynamic pore network model, modeling results presented in Figures 11a–11o demonstrate that the interfacial pattern in spontaneous imbibition remains consistent across pore networks with varying pore sizes but identical pore topology. Notably, this pattern is predominantly governed by the fluid viscosity ratio. Quantitative parameters, including Euler number and wetting-fluid saturation, were calculated, yielding relative errors of 5.5% and 6%, respectively, under various pore sizes, as depicted in Figure 11q. Consequently, the variation in pore size within networks of identical pore topology exerts only a marginal impact on spontaneous imbibition in single permeable media. The interfacial dynamics observed in spontaneous imbibition in single permeable media can thus serve as a control group, facilitating an exploration of the influence of flux exchange between dual permeable zones on displacement behaviors prompted by permeability ratios in dual-permeable media.

To investigate the influence of permeability contrast on spontaneous imbibition in dual-permeable media, we define the ratio of permeability in the high-permeable zone to that in the low-permeable zone as $C = K_1/K_2$. In the modified pore networks, the permeability in the high-permeable zone (K_1) remains constant, while the

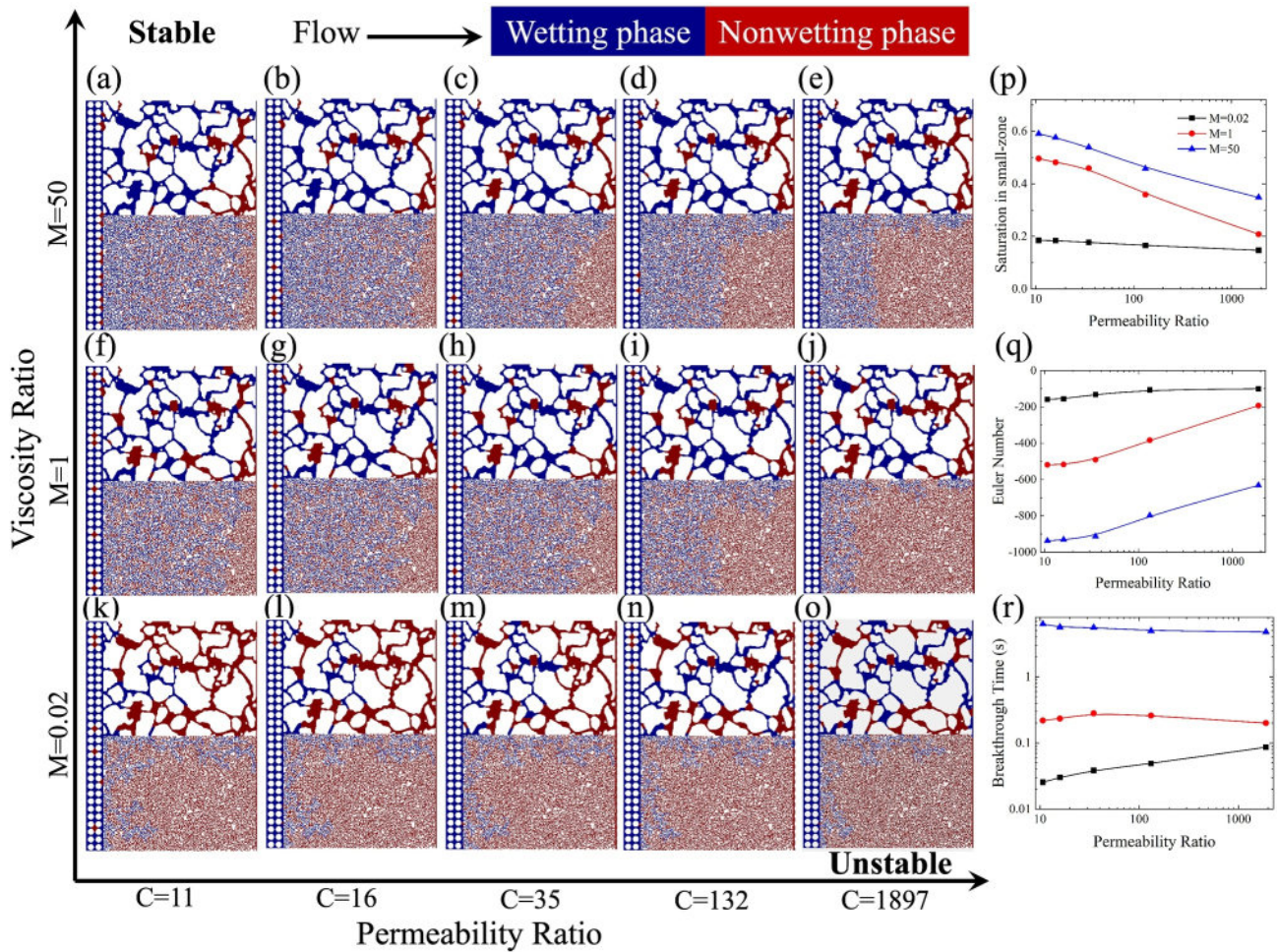


Figure 12. Impact of permeability ratio on spontaneous imbibition in dual permeable media: Interfacial pattern at breakthrough state under various permeability ratios and viscosity ratios (a–o), and the induced variation on wetting-fluid saturation in low-permeable zone (p), Euler Number (q), and the breakthrough time (r).

permeability in the low-permeable zone (K_2) varies from 0.29 μD to 57.5 μD . The permeability ratios (C) for the modified pore networks are 11, 16, 35, 132, and 1897. Employing the dynamic pore network model, we simulate spontaneous imbibition within the modified pore networks, and the modeling results for simulations with various viscosity ratios and permeability ratios are summarized in Figure 12.

Our primary focus is on the transient state when the wetting fluid breaks through the outlet in the low-permeable zone. In Figures 12a–12o, a comparison of interfacial patterns in each row underscores the significant impact of permeability ratio on spontaneous imbibition, contrasting with results obtained in single-permeable media (Figures 11a–11o). The interfacial pattern transitions from a stable type under low permeability ratio and high viscosity ratio to an unstable distribution under high permeability ratio and low viscosity ratio. This transition is attributed to the variation in flux exchange in dual-permeable media, resulting in a notable impact on wetting-fluid saturation in the low-permeable zone. Quantitative results are presented in Figures 12p–12r, revealing a monotonic decrease in wetting-fluid saturation and a monotonic increase in Euler number as the permeability ratio in the dual-permeable zone increases. Notably, a transition in the varying trend is observed between breakthrough time and permeability ratio as the fluid viscosity ratio increases. This phenomenon can be attributed to two factors: (1) an increasing permeability ratio tends to induce a transition in the interfacial pattern from a stable type to an unstable distribution, enhancing fluid invasion in the low-permeable zone; and (2) when the fingering pattern in the low-permeable zone becomes unstable enough under a high permeability ratio, the enhancement of fluid invasion velocity is suppressed.

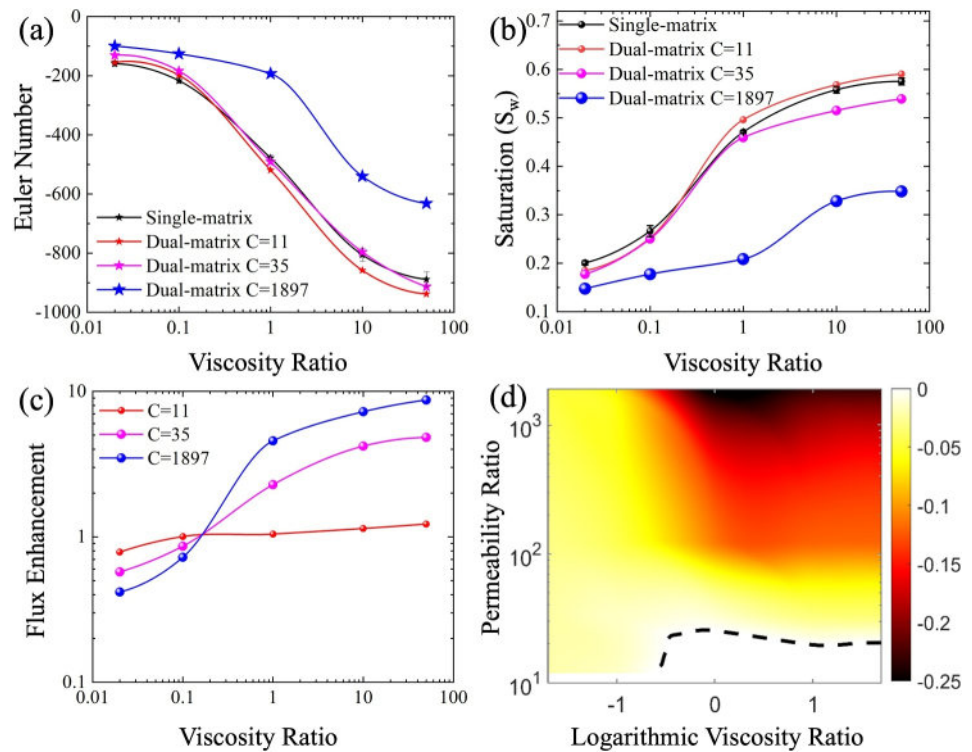


Figure 13. The impact of flux exchange during spontaneous imbibition at breakthrough in the dual permeable media: (a) Euler number variation; (b) Saturation variation; (c) Variation of flux enhancement; and (d) Variation of displacement efficiency.

3.2.2. The Displacement Efficiency Variation in Dual Permeable Media

The simulations conducted using the dynamic pore network model have elucidated that the permeability variation in the low permeable zone exerts a marginal impact on spontaneous imbibition in single-permeable media, while it significantly influences the interfacial pattern in dual-permeable media. In this section, we aim to investigate the effect of flux exchange in dual-permeable media on spontaneous imbibition under various permeability ratios. The analysis of quantitative parameters, including wetting-fluid saturation, Euler number, and flux enhancement in single- and dual-permeable media, provides a deeper understanding of the fluid invasion process in porous media, as depicted in Figure 13. The flux enhancement is defined as the ratio of the total flux from outlet pores in the low-permeable zone of dual-permeable media to that in single-permeable media. The variation of displacement efficiency is represented by the difference in wetting-fluid saturation between single- and dual-permeable media. In the modified pore networks with diverse pore sizes, the fluid viscosity ratio exhibits a similar impact during spontaneous imbibition—monotonic increase with wetting-fluid saturation, monotonic decrease with Euler number, and monotonic increase with flux enhancement.

The interfacial pattern tends toward a stable pattern (Euler number decreases with permeability ratio) under low permeability ratio and reaches an unstable pattern (Euler number increases with permeability ratio), as illustrated in Figure 13a, compared to the results in single-permeable media. Consequently, the transition of interfacial patterns leads to a similar change in wetting-fluid saturation—increasing under low permeability ratio and decreasing under high permeability ratio, as shown in Figure 13b.

The fluid flux exchange in dual-permeable media significantly contributes to the variation in spontaneous imbibition compared with multiphase flow in single-permeable media. Figure 13c demonstrates that the flux enhancement coefficient is smaller than 1 under unfavorable viscosity ratio ($M < 1$). This is attributed to the displaced fluid (nonwetting fluid) flowing into the high-permeable zone rather than into the outlet pores of the low-permeable zone. This flux exchange necessitates the wetting fluid to predominantly invade the pores near the high-permeable zone, resulting in a pronounced fingering pattern and lower wetting-fluid saturation in dual-

permeable media. Under favorable viscosity ratio ($M \geq 1$), more wetting fluid flows from the high-permeable zone into the low-permeable zone, leading to an enhancement of fluid flux in the low-permeable zone. This enhancement makes the spontaneous imbibition more stable under low permeability ratio. The substantial permeability contrast results in large viscous resistance and flow heterogeneity in dual-permeable media, inducing interfacial instability and transitioning fluid invasion from a stable displacement pattern to an unstable fingering pattern in the low-permeable zone. The displacement variation caused by flux exchange in dual-permeable media results in a notable difference in displacement efficiency under high viscosity ratio. To describe the impact of viscosity ratio and permeability ratio on spontaneous imbibition in single- and dual-permeable media, the phase diagram of the displacement efficiency variation was created in Figure 13d. The predominantly occupied regions, labeled as neglective parts, indicate that the displacement efficiency in dual-permeable media is smaller than that in single-permeable media, which indicates that the generation of high permeable zone during fracturing could reduce the oil recovery while it can provide a more economic production by enhancing the hydrocarbon flux in the low permeable zone. A dashed black line delineates the regions where the displacement efficiency variation is larger than zero and the oil recovery in low permeable zone of shale reservoir can be enhanced under low permeability ratio and high viscosity ratio. These findings could provide a theoretical guidance of the exploitation strategies for the choice of injecting fluid for the enhanced oil recovery.

4. Conclusions

In summary, our study investigates the displacement behavior during spontaneous imbibition in dual permeable media with permeability contrast. Simultaneously, we discuss the interfacial pattern of immiscible fluids under various viscosity ratios and permeability ratios. Employing the dynamic pore network model, our findings underscore the crucial role of flux exchange in comprehending multiphase flow dynamics within dual permeable media. Notably, it is essential to improve the pore doublet model by considering the flux exchange between the two channels when addressing the multiphase flow in dual permeable porous media.

Our theoretical analysis denotes an enhancement of fluid flow under favorable viscosity ratio and a reduction of fluid flow under unfavorable viscosity ratio in the low permeable zone of the dual permeable media due to flux exchange, which matches the modeling results for a comparison of spontaneous imbibition in a single permeable media with low permeability and dual permeable media. Furthermore, our observations highlight the transition of the interfacial pattern from stable displacement to unstable fingering as the viscosity ratio decreased, with larger permeability contrasts intensifying interfacial instability in dual permeable media. These insights contribute to an enhanced understanding of how flux exchange between neighboring porous zones influences imbibition preference and displacement efficiency in dual permeable media, emphasizing its dependency not only on fluid viscosity ratios but also on the permeability contrast of porous structures.

It is worth note that our simulations of spontaneous imbibition focus on moderate wettability ($\theta = 60^\circ$), with the dynamic pore network model considering only the main-meniscus interface. Previous research has demonstrated that wettability significantly affects multiphase displacement in porous media, manifesting distinct microscopic and macroscopic consequences under various wettability conditions (Holtzman & Segre, 2015; Lan et al., 2020; Lei, Gong, et al., 2023; Lei, Lu, et al., 2022). A comprehensive phase diagram capturing the interfacial pattern of multiphase flow, incorporating impacts from viscosity ratio, capillary number, and wetting conditions, necessitates further research efforts.

Appendix A: The Theoretical Solution of Spontaneous Imbibition in a Square Tube With Various Cross-Section Size

The square capillary tube with varying cross-section is shown in Figure 3, in which the radius and length of large zone are $R_b = 50 \mu\text{m}$ and $l_b = 100 \mu\text{m}$, and the values of small zone are $R_t = 10 \mu\text{m}$ and $l_t = 100 \mu\text{m}$. The tube length is $L = 1800 \mu\text{m}$. The fluid properties are the same as that in the square tube with identical cross-section. Thus, the time for invading the capillary tube with length l is.

$$(1) M = 0.001$$

$$t_i = t_{i-1} + \Delta t \quad (i = 1, 2, \dots, N)$$

$$\Delta t = \begin{cases} \frac{4R_t^2}{\Delta P - 2\sigma \cos \theta/R_t} \left(\frac{L - i * (l_b + l_t)}{\hat{g}} l - \frac{l^2}{2\hat{g}_t} \right) & 0 < l \leq \frac{lt}{2} \\ \frac{4R_b^2}{\Delta P - 2\sigma \cos \theta/R_b} \left(\frac{L - i * (l_b + l_t)}{\hat{g}} l - \frac{l_t l}{2\hat{g}_t} - \frac{l^2}{2\hat{g}_b} \right) & \frac{l_t}{2} < l \leq \frac{l_t}{2} + l_b \\ \frac{4R_t^2}{\Delta P - 2\sigma \cos \theta/R_t} \left(\frac{L - i * (l_b + l_t)}{\hat{g}} l - \frac{l_b l}{\hat{g}_b} - \frac{l_t l + l^2}{2\hat{g}_t} \right) & \frac{l_t}{2} + l_b < l \leq l_t + l_b \end{cases}$$

$$t_0 = 1$$

$$L = N * (l_t + l_b)$$

$$\hat{g} = \frac{0.5623}{\mu_{oil}(R_t^{-4} + R_b^{-4})}$$

$$\hat{g}_t = \frac{0.5623R_t^4}{\mu_{oil}}$$

$$\hat{g}_b = \frac{0.5623R_b^4}{\mu_{oil}}$$

(2) $M = 1$

$$\Delta t = \begin{cases} \frac{4R_t^2}{\Delta P - 2\sigma \cos \theta/R_t} \frac{Ll}{\hat{g}} & 0 < l \leq \frac{lt}{2} \\ \frac{4R_b^2}{\Delta P - 2\sigma \cos \theta/R_b} \frac{Ll}{\hat{g}} & \frac{l_t}{2} < l \leq \frac{l_t}{2} + l_b \\ \frac{4R_t^2}{\Delta P - 2\sigma \cos \theta/R_t} \frac{Ll}{\hat{g}} & \frac{l_t}{2} + l_b < l \leq l_t + l_b \end{cases}$$

(3) $M = 1000$

$$\Delta t = \begin{cases} \frac{4R_t^2}{\Delta P - 2\sigma \cos \theta/R_t} \left(\frac{i * (l_b + l_t)}{\hat{g}} l + \frac{l^2}{2\hat{g}_t} \right) & 0 < l \leq \frac{lt}{2} \\ \frac{4R_b^2}{\Delta P - 2\sigma \cos \theta/R_b} \left(\frac{i * (l_b + l_t)}{\hat{g}} l + \frac{l_t l}{2\hat{g}_t} + \frac{l^2}{2\hat{g}_b} \right) & \frac{l_t}{2} < l \leq \frac{l_t}{2} + l_b \\ \frac{4R_t^2}{\Delta P - 2\sigma \cos \theta/R_t} \left(\frac{i * (l_b + l_t)}{\hat{g}} l + \frac{l_b l}{\hat{g}_b} + \frac{l_t l + l^2}{2\hat{g}_t} \right) & \frac{l_t}{2} + l_b < l \leq l_t + l_b \end{cases}$$

Appendix B: The Experimental Validation of Multiphase Flow in Porous Media Using Dynamic Pore Network Model

The algorithm of dynamic pore network model is introduced in Section 2.2 and its validation is performed by comparing the imbibition behaviors from modeling and microfluidic experiment in the complex porous medium with micrometer size. The effective porosity and permeability of the rock sample are measured experimentally as 45% and 1.02 D. The sample size is cropped with height 6 mm and width 8 mm. The contact angle of water-oil in the microfluidic model is measured as 67°. The water-oil imbibition experiment in porous media was conducted under a constant capillary number ($Ca = \mu_w u / \sigma = 2 \times 10^{-5}$) and viscosity ratio ($M = \mu_w / \mu_n = 1.3$). The total

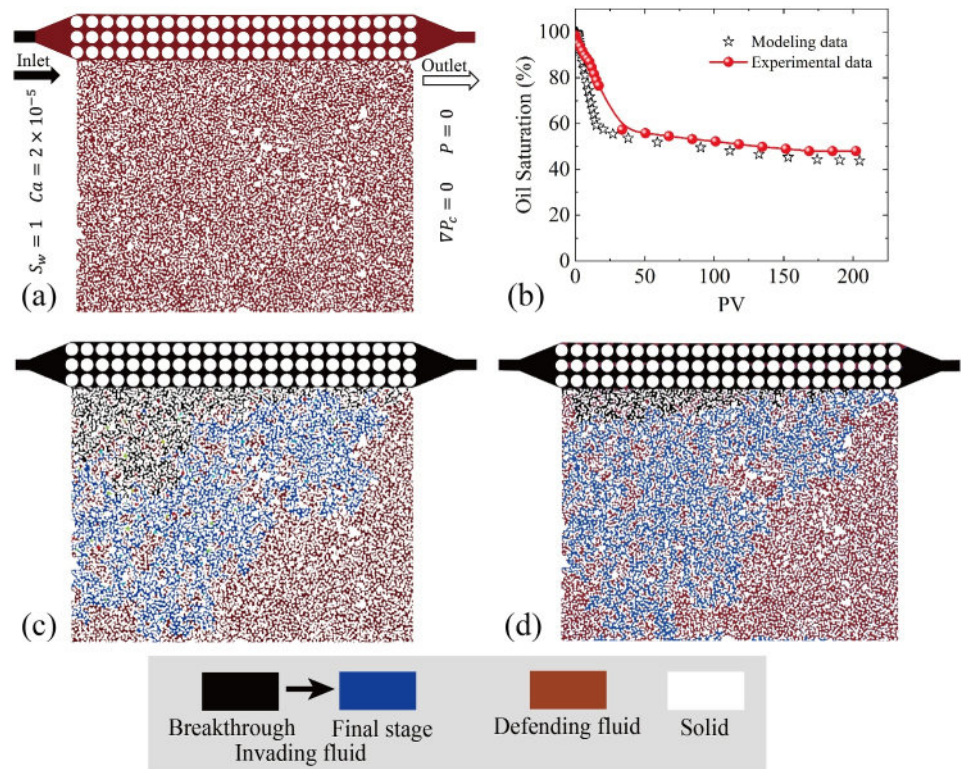


Figure B1. The validation of dynamic pore network model using the microfluidic experiment: (a) numerical conditions of water-oil imbibition with contact angle 67° in porous media using the dynamic pore network model (black part stands for water phase and red part for oil phase); (b) temporary variation of oil saturation for modeling and experimental data; interfacial patterns at breakthrough state and final state for dynamic pore network model and (c) microfluidic experiment (d).

injected fluid volume in experiment reached approximately 200 PV (about 7 hr) to ensure a final stable phase saturation. The dynamic pore network model of water-oil imbibition was performed under the same capillary number and viscosity ratio. The inlet and outlet pores are set as velocity and pressure boundary conditions, respectively, as shown in Fig. B1a. The oil saturation in the microfluidic model was extracted experimentally by calculating the space percentage of oil phase in the whole pore space during the imbibition process, and obtained numerically by computing the ratio of water volume to the whole pore space in the digital rock:

$$S_w = \frac{\sum_i V_i S_{w,i}}{\sum_i V_i} \quad (\text{B1})$$

Comparison of temporary variation of oil saturation during imbibition process in porous media from experimental and modeling results, as shown in Fig. B1b, demonstrated that the dynamic pore network model in this study could predict well the imbibition evolution of multiphase flow in the complex pore system. Moreover, both modeling and experimental results (Fig B1c and B1d) indicate that the water phase almost invades the pores along the preferential path in porous media before breakthrough state, and much oil phase in the matrix pores are displaced in subsequent process when the water phase fluxes from the pores in the preferential path into the matrix pores.

Data Availability Statement

The code in this work is implemented on the open-source software MATLAB Reservoir Simulation Toolbox (MRST) developed primarily by the Applied Computational Science group in the Department of Mathematics and Cybernetics at SINTEF Digital (Bao, 2017). The library is available at <https://www.sintef.no/projectweb/mrst/>.

Acknowledgments

This work is financially supported by the NSF grant of China (No. 12272207) and the National Key Research and Development Program of China (No. 2019YFA0708704).

References

Aguilar-López, J. P., Bogaard, T., & Gerke, H. H. (2020). Dual-permeability model Improvements for representation of preferential flow in fractured Clays. *Water Resources Research*, *56*(8), e2020WR027304. <https://doi.org/10.1029/2020WR027304>

Akhlaghi Amiri, H. A., & Hamouda, A. A. (2014). Pore-scale modeling of non-isothermal two-phase flow in 2D porous media: Influences of viscosity, capillarity, wettability and heterogeneity. *International Journal of Multiphase Flow*, *61*, 14–27. <https://doi.org/10.1016/j.ijmultiphaseflow.2014.01.001>

An, S., Erfani, H., Godínez-Brizuela, O. E., & Niasar, V. (2020). Transition from viscous fingering to capillary fingering: Application of GPU-based fully implicit dynamic pore network modeling. *Water Resources Research*, *56*(12), e2020WR028149. <https://doi.org/10.1029/2020WR028149>

Armstrong, R. T., & Berg, S. (2013). Interfacial velocities and capillary pressure gradients during Haines jumps. *Physical Review E*, *88*(4), 043010. <https://doi.org/10.1103/PhysRevE.88.043010>

Arshadi, M., Khishvand, M., Aghaei, A., Piri, M., & Al-Muntasher, G. A. (2018). Pore-scale experimental investigation of two-phase flow through fractured porous media. *Water Resources Research*, *54*(5), 3602–3631. <https://doi.org/10.1029/2018WR022540>

Bakhshian, S., Murakami, M., Hosseini, S. A., & Kang, Q. (2020). Scaling of imbibition front dynamics in heterogeneous porous media. *Geophysical Research Letters*, *47*(14), e2020GL087914. <https://doi.org/10.1029/2020GL087914>

Bao, K. (2017). The MATLAB reservoir simulation Toolbox: March 21, 2022 Release (Version MRST 2022a) [Software]. *MRST*. <https://www.sintef.no/projectweb/mrst/>

Blunt, M. J., Jackson, M. D., Piri, M., & Valvatne, P. H. (2002). Detailed physics, predictive capabilities and macroscopic consequences for pore-network models of multiphase flow. *Advances in Water Resources*, *25*(8), 1069–1089. [https://doi.org/10.1016/S0309-1708\(02\)00049-0](https://doi.org/10.1016/S0309-1708(02)00049-0)

Cha, L., Xie, C., Feng, Q., & Balhoff, M. (2021). Geometric Criteria for the snap-off of a non-wetting Droplet in pore-throat channels with Rectangular cross-sections. *Water Resources Research*, *57*(7), e2020WR029476. <https://doi.org/10.1029/2020WR029476>

Chatzis, I., & Dullien, F. A. L. (1983). Dynamic immiscible displacement mechanisms in pore doublets: Theory versus experiment. *Journal of Colloid and Interface Science*, *91*(1), 199–222. [https://doi.org/10.1016/0021-9797\(83\)90326-0](https://doi.org/10.1016/0021-9797(83)90326-0)

Chen, S., & Guo, B. (2023). Pore-scale modeling of PFAS transport in water-Unsaturated porous media: Air–water interfacial Adsorption and mass-Transfer processes in thin water Films. *Water Resources Research*, *59*(8), e2023WR034664. <https://doi.org/10.1029/2023WR034664>

Chen, S., Jiang, J., & Guo, B. (2021). A pore-network-based upscaling framework for the nanoconfined phase behavior in shale rocks. *Chemical Engineering Journal*, *417*, 129210. <https://doi.org/10.1016/j.cej.2021.129210>

Chen, S., Qin, C., & Guo, B. (2020). Fully implicit dynamic pore-network modeling of two-phase flow and phase change in porous media. *Water Resources Research*, *56*(11), e2020WR028510. <https://doi.org/10.1029/2020WR028510>

Chen, Y., Valocchi, A. J., Kang, Q., & Viswanathan, H. S. (2019). Inertial effects during the process of Supercritical CO₂ displacing brine in a sandstone: Lattice Boltzmann simulations based on the Continuum-surface-force and geometrical wetting models. *Water Resources Research*, *55*(12), 11144–11165. <https://doi.org/10.1029/2019WR025746>

Choi, E. S., Cheema, T., & Islam, M. R. (1997). A new dual-porosity/dual-permeability model with non-Darcian flow through fractures. *Journal of Petroleum Science and Engineering*, *17*(3), 331–344. [https://doi.org/10.1016/S0920-4105\(96\)00050-2](https://doi.org/10.1016/S0920-4105(96)00050-2)

Cieplak, M., & Robbins, M. O. (1988). Dynamical transition in quasistatic fluid invasion in porous media. *Physical Review Letters*, *60*(20), 2042–2045. <https://doi.org/10.1103/PhysRevLett.60.2042>

Cieplak, M., & Robbins, M. O. (1990). Influence of contact angle on quasistatic fluid invasion of porous media. *Physical Review B*, *41*(16), 11508–11521. <https://doi.org/10.1103/PhysRevB.41.11508>

Gao, Y., Raeini, A. Q., Blunt, M. J., & Bijeljic, B. (2021). Dynamic fluid configurations in steady-state two-phase flow in Bentheimer sandstone. *Physical Review E*, *103*(1), 013110. <https://doi.org/10.1103/PhysRevE.103.013110>

Gerke, H. H., Dusek, J., & Vogel, T. (2013). Solute mass Transfer effects in two-dimensional dual-permeability modeling of Bromide Leaching from a Tile-Drained field. *Vadose Zone Journal*, *12*(2), 1–21. <https://doi.org/10.2136/vzj2012.0091>

Gu, Q., Liu, H., & Wu, L. (2021). Preferential imbibition in a dual-permeability pore network. *Journal of Fluid Mechanics*, *915*, A138. <https://doi.org/10.1017/jfm.2021.174>

Han, T., Gurevich, B., Fu, L.-Y., Qi, Q., Wei, J., & Chen, X. (2020). Combined effects of pressure and water saturation on the Seismic anisotropy in Artificial porous sandstone with aligned fractures. *Journal of Geophysical Research: Solid Earth*, *125*(1), e2019JB019091. <https://doi.org/10.1029/2019JB019091>

He, Z., Liang, F., & Meng, J. (2022). Pore-scale study of the effect of bifurcated fracture on spontaneous imbibition in heterogeneous porous media. *Physics of Fluids*, *34*(7), 072003. <https://doi.org/10.1063/5.0095553>

Holtzman, R., & Segre, E. (2015). Wettability Stabilizes fluid invasion into porous media via Nonlocal, cooperative pore filling. *Physical Review Letters*, *115*(16), 164501. <https://doi.org/10.1103/PhysRevLett.115.164501>

Hu, R., Lan, T., Wei, G.-J., & Chen, Y.-F. (2019). Phase diagram of quasi-static immiscible displacement in disordered porous media. *Journal of Fluid Mechanics*, *875*, 448–475. <https://doi.org/10.1017/jfm.2019.504>

Huan, X., Zhang, R., Qian, J., Ma, L., Fang, Y., & Yan, Y. (2024). Introducing a transition domain for describing the solute exchange between macropores/fractures and matrix in dual-permeability system. *Journal of Hydrology*, *634*, 131130. <https://doi.org/10.1016/j.jhydrol.2024.131130>

Joekar-Niasar, V., & Hassanzadeh, S. M. (2012). Analysis of fundamentals of two-phase flow in porous media using dynamic pore-network models: A review. *Critical Reviews in Environmental Science and Technology*, *42*(18), 1895–1976. <https://doi.org/10.1080/10643389.2011.574101>

Lan, T., Hu, R., Yang, Z., Wu, D.-S., & Chen, Y.-F. (2020). Transitions of fluid invasion patterns in porous media. *Geophysical Research Letters*, *47*(20), e2020GL089682. <https://doi.org/10.1029/2020GL089682>

Legland, D., Arganda-Carreras, I., & Andrey, P. (2016). MorphoLibJ: Integrated library and plugins for mathematical morphology with ImageJ. *Bioinformatics*, *32*(22), 3532–3534. <https://doi.org/10.1093/bioinformatics/btw413>

Lei, W., Gong, W., Lu, X., & Wang, M. (2024). Fluid entrapment during forced imbibition in a multidepth microfluidic chip with complex porous geometry. *Journal of Fluid Mechanics*, *987*, A3. <https://doi.org/10.1017/jfm.2024.358>

Lei, W., Gong, W., & Wang, M. (2023a). Wettability effect on displacement in disordered media under preferential flow conditions. *Journal of Fluid Mechanics*, *975*, A33. <https://doi.org/10.1017/jfm.2023.879>

Lei, W., Li, Q., Yang, H.-E., Wu, T.-J., Wei, J., & Wang, M. (2022a). Preferential flow control in heterogeneous porous media by concentration-manipulated rheology of microgel particle suspension. *Journal of Petroleum Science and Engineering*, *212*, 110275. <https://doi.org/10.1016/j.petrol.2022.110275>

- Lei, W., Lu, X., Gong, W., & Wang, M. (2023b). Triggering interfacial instabilities during forced imbibition by adjusting the aspect ratio in depth-variable microfluidic porous media. *Proceedings of the National Academy of Sciences*, 120(50), e2310584120. <https://doi.org/10.1073/pnas.2310584120>
- Lei, W., Lu, X., Liu, F., & Wang, M. (2022b). Non-monotonic wettability effects on displacement in heterogeneous porous media. *Journal of Fluid Mechanics*, 942, R5. <https://doi.org/10.1017/jfm.2022.386>
- Lenormand, R., Touboul, E., & Zarcone, C. (1988). Numerical models and experiments on immiscible displacements in porous media. *Journal of Fluid Mechanics*, 189, 165–187. <https://doi.org/10.1017/S0022112088000953>
- Lenormand, R., Zarcone, C., & Sarr, A. (1983). Mechanisms of the displacement of one fluid by another in a network of capillary ducts. *Journal of Fluid Mechanics*, 135, 337–353. <https://doi.org/10.1017/s0022112083003110>
- Liu, F., & Wang, M. (2020). Review of low salinity waterflooding mechanisms: Wettability alteration and its impact on oil recovery. *Fuel*, 267, 117112. <https://doi.org/10.1016/j.fuel.2020.117112>
- Liu, F., & Wang, M. (2022). Phase diagram for preferential flow in dual permeable media. *Journal of Fluid Mechanics*, 948, A19. <https://doi.org/10.1017/jfm.2022.649>
- Liu, Y., Gong, W., Zhao, Y., Jin, X., & Wang, M. (2022). A pore-throat segmentation method based on local hydraulic resistance equivalence for pore-network modeling. *Water Resources Research*, 58(12), e2022WR033142. <https://doi.org/10.1029/2022WR033142>
- Mathia, E. J., Rexer, T. F. T., Thomas, K. M., Bowen, L., & Aplin, A. C. (2019). Influence of Clay, Calcareous Microfossils, and Organic Matter on the nature and Diagenetic evolution of pore systems in Mudstones. *Journal of Geophysical Research: Solid Earth*, 124(1), 149–174. <https://doi.org/10.1029/2018JB015941>
- Moore, T. F., & Slobod, R. L. (1955). Displacement of oil by water-effect of wettability, rate, and viscosity on recovery. Fall Meeting of the Petroleum Branch of AIME. <https://doi.org/10.2118/502-G>
- Muljadi, B. P., Blunt, M. J., Raeni, A. Q., & Bijeljic, B. (2016). The impact of porous media heterogeneity on non-Darcy flow behaviour from pore-scale simulation. *Advances in Water Resources*, 95, 329–340. <https://doi.org/10.1016/j.advwatres.2015.05.019>
- Øren, P. E., Bakke, S., & Arntzen, O. J. (1998). Extending predictive capabilities to network models. *SPE Journal*, 3(4), 324–336. <https://doi.org/10.2118/52052-pa>
- Patzek, T. W., & Silin, D. B. (2001). Shape factor and hydraulic conductance in Noncircular Capillaries: I. One-phase creeping flow. *Journal of Colloid and Interface Science*, 236(2), 295–304. <https://doi.org/10.1006/jcis.2000.7413>
- Primkulov, B. K., Pahlavan, A. A., Fu, X., Zhao, B., MacMinn, C. W., & Juanes, R. (2021). Wettability and Lenormand's diagram. *Journal of Fluid Mechanics*, 923, A34. <https://doi.org/10.1017/jfm.2021.579>
- Qin, C.-Z., Guo, B., Celia, M., & Wu, R. (2019). Dynamic pore-network modeling of air-water flow through thin porous layers. *Chemical Engineering Science*, 202, 194–207. <https://doi.org/10.1016/j.ces.2019.03.038>
- Qin, C.-Z., & van Brummelen, H. (2019). A dynamic pore-network model for spontaneous imbibition in porous media. *Advances in Water Resources*, 133, 103420. <https://doi.org/10.1016/j.advwatres.2019.103420>
- Qin, C.-Z., Wang, X., Hefny, M., Zhao, J., Chen, S., & Guo, B. (2022). Wetting dynamics of spontaneous imbibition in porous media: From pore scale to Darcy scale. *Geophysical Research Letters*, 49(4), e2021GL097269. <https://doi.org/10.1029/2021GL097269>
- Rabbani, H. S., Or, D., Liu, Y., Lai, C.-Y., Lu, N. B., Datta, S. S., et al. (2018). Suppressing viscous fingering in structured porous media. *Proceedings of the National Academy of Sciences*, 115(19), 4833–4838. <https://doi.org/10.1073/pnas.1800729115>
- Rothman, D. H. (1990). Macroscopic laws for immiscible two-phase flow in porous media: Results from numerical experiments. *Journal of Geophysical Research*, 95(B6), 8663–8674. <https://doi.org/10.1029/JB095B06p08663>
- Shan, F., Chai, Z., Shi, B., & Zhao, M. (2023). Optimal displacement of immiscible two-phase fluids in a pore doublet. *Physics of Fluids*, 35(5), 053332. <https://doi.org/10.1063/5.0149182>
- Siddiqui, M. A. Q., Ali, S., Fei, H., & Roshan, H. (2018). Current understanding of shale wettability: A review on contact angle measurements. *Earth-Science Reviews*, 181, 1–11. <https://doi.org/10.1016/j.earscirev.2018.04.002>
- Wang, F., Xu, H., Liu, Y., Meng, X., & Liu, L. (2023). Mechanism of low Chemical Agent Adsorption by high pressure for hydraulic fracturing-Assisted oil displacement Technology: A study of molecular dynamics combined with Laboratory experiments. *Langmuir*, 39(46), 16628–16636. <https://doi.org/10.1021/acs.langmuir.3c02634>
- Wang, Z., Chauhan, K., Pereira, J.-M., & Gan, Y. (2019). Disorder characterization of porous media and its effect on fluid displacement. *Physical Review Fluids*, 4(3), 034305. <https://doi.org/10.1103/PhysRevFluids.4.034305>
- Wu, K., Chen, Z., Li, J., Lei, Z., Xu, J., Wang, K., et al. (2019). Nanoconfinement effect on n-Alkane flow. *Journal of Physical Chemistry C*, 123(26), 16456–16461. <https://doi.org/10.1021/acs.jpcc.9b03903>
- Wu, K., Chen, Z., Li, J., Li, X., Xu, J., & Dong, X. (2017). Wettability effect on nanoconfined water flow. *Proceedings of the National Academy of Sciences*, 114(13), 3358–3363. <https://doi.org/10.1073/pnas.1612608114>
- Xie, C., Lei, W., Balhoff, M. T., Wang, M., & Chen, S. (2021). Self-adaptive preferential flow control using displacing fluid with dispersed polymers in heterogeneous porous media. *Journal of Fluid Mechanics*, 906, A10. <https://doi.org/10.1017/jfm.2020.763>
- Zhang, C., Oostrom, M., Grate, J. W., Wietsma, T. W., & Warner, M. G. (2011). Liquid CO₂ displacement of water in a dual-permeability pore network Micromodel. *Environmental Science & Technology*, 45(17), 7581–7588. <https://doi.org/10.1021/es201858r>
- Zhang, Y., Bijeljic, B., Gao, Y., Lin, Q., & Blunt, M. J. (2021). Quantification of nonlinear multiphase flow in porous media. *Geophysical Research Letters*, 48(5), e2020GL090477. <https://doi.org/10.1029/2020GL090477>
- Zhao, B., MacMinn, C. W., Primkulov, B. K., Chen, Y., Valocchi, A. J., Zhao, J., et al. (2019). Comprehensive comparison of pore-scale models for multiphase flow in porous media. *Proceedings of the National Academy of Sciences*, 116(28), 13799–13806. <https://doi.org/10.1073/pnas.1901619116>
- Zheng, J., Ju, Y., & Wang, M. (2018). Pore-scale modeling of spontaneous imbibition behavior in a complex shale porous structure by Pseudopotential lattice Boltzmann method. *Journal of Geophysical Research: Solid Earth*, 123(11), 9586–9600. <https://doi.org/10.1029/2018JB016430>
- Zheng, J., Wang, Z., Ju, Y., Tian, Y., Jin, Y., & Chang, W. (2021). Visualization of water channeling and displacement diversion by polymer gel treatment in 3D printed heterogeneous porous media. *Journal of Petroleum Science and Engineering*, 198, 108238. <https://doi.org/10.1016/j.petrol.2020.108238>